Fermilab

Recoil-Safe Subtraction, Matching and Merging in e+e- to hadrons

FERMILAB-PUB-25-0479-T

arXiv:2507.22837

FERMILAB-PUB-25-0479-T, IPPP-25-49, ZU-TH 49/25, CERN-TH-2025-141, MCNET-25-18

Recoil-Safe Subtraction, Matching and Merging in $e^+e^-\to$ hadrons

Stefan Höche,[1] Frank Krauss,[2] Peter Meinzinger,[3] and Daniel Reichelt[4]

[1] *Fermi National Accelerator Laboratory, Batavia, IL, 60510*
[2] *Institute for Particle Physics Phenomenology, Durham University, Durham DH1 3LE, UK*
[3] *Physik-Institut, Universität Zürich, CH-8057 Zürich, Switzerland*
[4] *Theoretical Physics Department, CERN, CH-1211 Geneva, Switzerland*

We present the first next-to-leading order matched and multi-jet merged predictions based on the Alaric parton shower. The components needed for infrared subtraction in the S-Mc@Nlo algorithm are computed analytically for the case of color singlet decays to hadronic final states and validated against existing approaches for up to $e^-e^+ \to 5$ jets. Phenomenological results for $e^-e^+ \to$ hadrons at the Z pole are obtained with up to five jets at next-to-leading order precision, for the first time using an evolution algorithm with NLL-preserving kinematics mapping.

I. INTRODUCTION

For more than four decades, parton-shower event generators have played an important role in deciphering the nature of elementary particles and their interactions [1, 2]. They provide a generic method to simulate the complete hadronic final states measured in collider experiments such as Atlas, Cms, LhcB or Alice at the Large Hadron Collider (LHC) at CERN [3–6]. They are also essential for the planning of future experiments such as those at a potential Future Circular Collider (FCC) [7–9]. Due to the high energies involved in these measurements, the correct description of QCD radiative effects plays a vital role. They are implemented in the simulation by parton shower algorithms, which have been a topic of intense research activity for many years [10–55]. The matching of parton showers to next-to-leading order (NLO) calculations [56–62], and the merging of calculations for varying jet multiplicity [63–79] are crucial for the success of searches for physics beyond the Standard Model, both in the form of direct limit setting, and in the form of precision measurements of known Standard Model quantities.

All existing fully differential matching algorithms are based on using the parton shower evolution kernels to create an approximate higher-order real-emission correction, which is then used to cancel the infrared singularities of the actual NLO real-emission contribution. When spin and color correlations are taken into account, the remainder of this subtraction is finite in four dimensions and can therefore be integrated out with Monte-Carlo methods. It is treated as a hard correction to the inclusive reaction, which means that it is a new type of contribution that cannot be described by the unitary parton evolution. The Mc@Nlo matching algorithm [56] provided the first fully differential, process-independent technique to include this hard correction in parton-level event generators.

This paper reports on the implementation of the S-Mc@Nlo matching for the Alaric parton-shower algorithm [47–49], and on the creation of a fixed-order subtraction that mirrors the parton-shower up to first order in the strong coupling. This is achieved by re-purposing relevant results of massless and massive Catani-Seymour dipole subtraction [80, 81], in particular the solutions to the color algebra [82] and the phase-space parametrization for splittings with identified partons and with a massive spectator. The S-Mc@Nlo matching method accounts for both non-trivial color correlations and non-trivial spin correlations across the hard process and the first splitting by reweighting the parton shower with the relevant insertion operators on a point-by-point basis [61, 83].

While such matching methods are useful to correct the event simulation to the inclusive n-jet rate, and to correctly include the effects of a single hard emission, they fail to correctly model the often intricate effects of correlations among many hard, well-separated jets accompanying the inclusive process of interest. Such configurations require dedicated calculations for the many-jet final state, which can be included by multi-jet merging algorithms that exist both at leading [63–74] and at next-to-leading order [75–79] in QCD perturbation theory. We therefore also report on the implementation of MePs@Nlo [76, 77], a next-to-leading-order accurate merging technique, for the Alaric parton shower. It allows us to make the first NLO-accurate predictions using a parton shower with a NLL-safe recoil scheme for observables sensitive to three-, four- and five-jet configurations in e^+e^- annihilation into hadrons. These results will be particularly useful to gauge the impact of higher-order corrections versus non-perturbative power corrections from hadronization in the region around the Sudakov shoulder of the thrust and C-parameter distribution.

This manuscript is organized as follows. Section II discusses the infrared subtraction method and presents the analytic expressions for the corresponding integrals. Section III contains the validation of the fixed-order calculations, and of the matching and merging procedures. Section IV presents the first phenomenological applications and discusses the impact of the higher-order corrections. Finally, Sec. V presents an outlook and discusses further steps towards precision simulations for the LHC and a potential FCC.

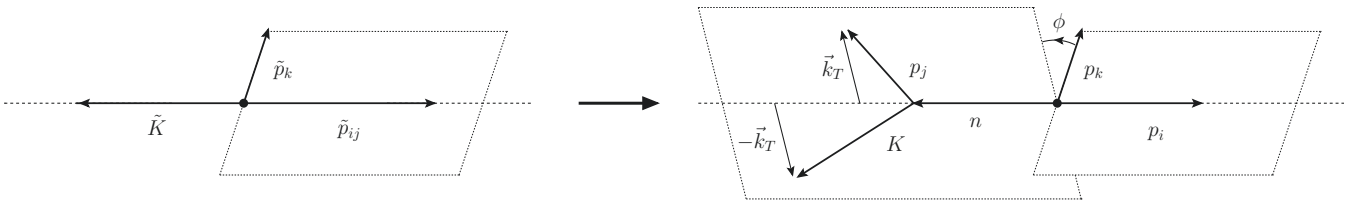

FIG. 1. Momentum assignment in radiation kinematics.

II. ANALYTIC RESULTS

We start with the derivation of the analytic integrals that are necessary for the construction of the fixed-order infrared subtraction scheme corresponding to the ALARIC parton shower. To this end, we use the ALARIC splitting functions and the kinematic mappings discussed in [48]; in particular we differentiate between scalar (soft) and splitting (collinear) kinematics, and we only address the case of massless final-state partons.

A. Scalar contribution

The infrared structure of the real-emission corrections with final-state partons can be described using the Catani-Seymour dipole factorization formulae [80, 81]:

$$ {}_{m+1}\langle 1,\dots,i,\dots,j,\dots,m+1|1,\dots,i,\dots,j,\dots,m+1\rangle_{m+1} = \sum_{k\neq a} \mathcal{D}_{ij,k}(p_1,\dots,p_{m+1}) \,, \tag{1}$$

where the individual dipole contribution is given by

$$ \mathcal{D}_{ij,k}(p_1,\dots,p_{m+1}) = -\frac{1}{2p_ip_j}\, {}_m\langle \tilde{1},\dots,\widetilde{ij},\dots,\widetilde{m+1}|\frac{\mathbf{T}_i\mathbf{T}_k}{\mathbf{T}_i^2}V_{ij,k}|\tilde{1},\dots,\widetilde{ij},\dots,\widetilde{m+1}\rangle_m \,. \tag{2}$$

We separate the differential insertion operator $V_{ij,k}$ into a partial fractioned scalar contribution and a pure splitting component, which are labeled with superscripts $^{(s)}$ and $^{(p)}$, respectively. They can also be interpreted as a soft and a collinear contribution [84]

$$ V_{ij,k} = V_{ij,k}^{(s)} + V_{ij,k}^{(p)} \,. \tag{3}$$

In complete analogy to the differential insertion operator, $V_{ij,k}$, we define the integral of its spin average over the one-emission phase space, $\mathbf{I}$, as a sum of soft and collinear components:

$$ \mathbf{I} = \int [\mathrm{d}p_j] \frac{1}{2p_ip_j}\langle V_{ij,k}\rangle = -\frac{\alpha_s}{2\pi}\frac{1}{\Gamma(1-\varepsilon)}\left(\frac{4\pi\mu^2}{s_{ik}}\right)^{\varepsilon}\frac{\mathbf{T}_{ij}\mathbf{T}_k}{\mathbf{T}_{ij}^2}\left(I_{i,k}^{(s)} + I_{ij}^{(p)}\right) \,, \tag{4}$$

where $s_{ik} = 2\tilde{p}_i\tilde{p}_k$, and where we follow the notation of Refs. [80, 81]. Note that the spin-averaged splitting function appears in this calculation due to a simplification of the azimuthal angle integrals over spin-dependent contributions. This constrains the form of the transverse vector used in the evaluation of the splitting functions, Eq. (16).

For splittings where the final-state parton i is not a gluon, the scalar components of Eq. (3) and (4) vanish. For all others, they are given by the differential and integrated form of the partial fractioned eikonal defined in the ALARIC parton-shower algorithm [47, 48].

$$ V_{ig,k}^{(s)}(p_i,p_j,n) = 8\pi\mu^{2\varepsilon}\alpha_s\, C_i\, \frac{2(p_ip_k)(p_in)}{(p_ip_j)(p_kn)+(p_kp_j)(p_in)} \,, \tag{5}$$

where C_i is the quadratic color Casimir operator of the emitting particle, i. The partial fractioned scalar insertion operators are spin-independent, i.e., they are diagonal in the spin states of any particle they act on. This is due to the fact that they represent the semi-classical component of the radiative corrections [85, 86].

The radiation kinematics are sketched in Fig. 1. The phase space is parameterized through the variables [47, 80]

$$ v = \frac{p_ip_j}{p_i\tilde{K}} \qquad \text{and} \qquad z = \frac{p_i\tilde{K}}{\tilde{p}_i\tilde{K}} \,. \tag{6}$$

The final-state momentum of the emitter, $\tilde{p}_i$, and the recoil momentum, $\tilde{K}$, are given by

$$\begin{aligned} p_i &= z\,\tilde{p}_i\ , \\ p_j &= (1-z)\,\tilde{p}_i + v\big(\tilde{K} - (1-z+2\kappa)\,\tilde{p}_i\big) - k_\perp\ , \\ K &= \tilde{K} - v\big(\tilde{K} - (1-z+2\kappa)\,\tilde{p}_i\big) + k_\perp\ , \end{aligned} \tag{7}$$

with the magnitude squared of the transverse momentum defined as

$$\mathrm{k}_\perp^2 = v(1-v)(1-z)\,2\tilde{p}_i\tilde{K} - v^2\tilde{K}^2\ . \tag{8}$$

For the final-state evolution of a single QCD multipole, the momentum $\tilde{K}$ is composed of the two initial-state momenta. In this case, all final-state momenta are subjected to the Lorentz transformation

$$p_l^\mu \to \Lambda^\mu_\nu(K,\tilde{K})\,p_l^\nu\ , \qquad \text{where} \qquad \Lambda^\mu_\nu(\tilde{K},K) = g^\mu_\nu - \frac{2(K+\tilde{K})^\mu(K+\tilde{K})_\nu}{(K+\tilde{K})^2} + \frac{2K^\mu\tilde{K}_\nu}{\tilde{K}^2}\ . \tag{9}$$

The integrated scalar insertion operator corresponds to the massless limit of Eq. (55) in [48]. We obtain

$$I_{ik}^{(s)} = \int_0^1 \mathrm{d}z \left(-\frac{\delta(1-z)}{2\varepsilon} + \frac{z}{[1-z]_+} - 2\varepsilon z \left[\frac{\log(1-z)}{1-z}\right]_+ \right) \tag{10}$$

$$\times\, 2z^{-\varepsilon}\left(\frac{np_k}{np_i}\right)^\varepsilon \frac{\Gamma^2(1-\varepsilon)}{\Gamma(1-2\varepsilon)} \left(\frac{1}{\varepsilon} + \varepsilon\,\mathrm{Li}_2\left(1 - \frac{n^2(p_ip_k)}{2(np_i)(np_k)}\right)\right)\ . \tag{11}$$

Note that n implicitly depends on z. Using the variables

$$\rho \equiv \frac{2\tilde{p}_k\tilde{K}}{s_{ik}}, \qquad \tau \equiv \frac{2\tilde{p}_i\tilde{K}}{s_{ik}}, \qquad \mu_K \equiv \frac{\tilde{K}^2}{s_{ik}}\ . \tag{12}$$

we can parametrize all scalar products in terms of the squared dipole mass $s_{ik} = 2\tilde{p}_i\tilde{p}_k$,

$$2np_i = z\tau s_{ik}, \qquad 2np_k = (1-z+\rho)s_{ik}, \qquad n^2 = \big[(1-z)\tau + \mu_K\big]\,s_{ik}\ . \tag{13}$$

The final result, again expanded up to $\mathcal{O}(\varepsilon^0)$, reads

$$\begin{aligned} I_{ik}^{(s)} = {} & \frac{1}{\varepsilon^2} + \frac{2}{\varepsilon} + \left(6 - \frac{\pi^2}{2}\right) + \frac{1}{2}\ln^2\left(\frac{\rho}{\tau}\right) + \mathrm{Li}_2\left(1 - \frac{\mu_K}{\rho\tau}\right) \\ & - 2\,\mathrm{Re}\left\{\mathrm{Li}_2\left(1+\frac{1}{\rho}\right)\right\} - 2\Big(1+\rho+\log|\rho|\Big)\log\frac{\rho+1}{\rho} + (\rho\leftrightarrow\tau)\ , \end{aligned} \tag{14}$$

where we have suppressed terms that do not contribute to the sum over the two legs i,k of a dipole due to symmetry. Note that in the simplest case of a color singlet decay to two jets, we would have $\tilde{K} = -\tilde{p}_i - \tilde{p}_k$ and hence $\rho = -1$, $\tau = -1$, $\mu_K = 1$. In this case, only the constant terms contribute to Eq. (14), and we obtain the standard soft integral for the massless case [80, 81].

B. Pure splitting remainders

The kinematics mapping used in the computation of pure splitting functions is sketched in Fig. 2. We define

$$Q^2 = 2\tilde{p}_i\tilde{K} + \tilde{K}^2, \qquad \hat{\kappa} = \frac{\tilde{K}^2}{Q^2}\ . \tag{15}$$

The insertion operators are given by the spin-dependent pure remainders of the DGLAP splitting functions [81, 84]

$$\begin{aligned} \langle s|V^{\mathrm{coll}}_{gq,k}|s'\rangle &= 8\pi\mu^{2\varepsilon}\alpha_s\,C_F\,\delta_{ss'}\,(1-\varepsilon)\,\tilde{z}_j\ , \\ \langle \mu|V^{\mathrm{coll}}_{q\bar{q},k}|\nu\rangle &= 8\pi\mu^{2\varepsilon}\alpha_s\,C_F\left\{ -g^{\mu\nu}\left[1 - \frac{2\,\eta\,z_+z_-}{1-\varepsilon}\right] - \frac{2}{p_ip_j}\Big[\tilde{z}_i^{(m)}p_i^\mu - \tilde{z}_j^{(m)}p_j^\mu\Big]\Big[\tilde{z}_i^{(m)}p_i^\nu - \tilde{z}_j^{(m)}p_j^\nu\Big]\right\}, \\ \langle \mu|V^{\mathrm{coll}}_{gg,k}|\nu\rangle &= 16\pi\mu^{2\varepsilon}\alpha_s\,C_A\left\{ -g^{\mu\nu}\,\eta\,z_+z_- + \frac{1-\varepsilon}{p_ip_j}\Big[\tilde{z}_i^{(m)}p_i^\mu - \tilde{z}_j^{(m)}p_j^\mu\Big]\Big[\tilde{z}_i^{(m)}p_i^\nu - \tilde{z}_j^{(m)}p_j^\nu\Big]\right\}, \end{aligned} \tag{16}$$

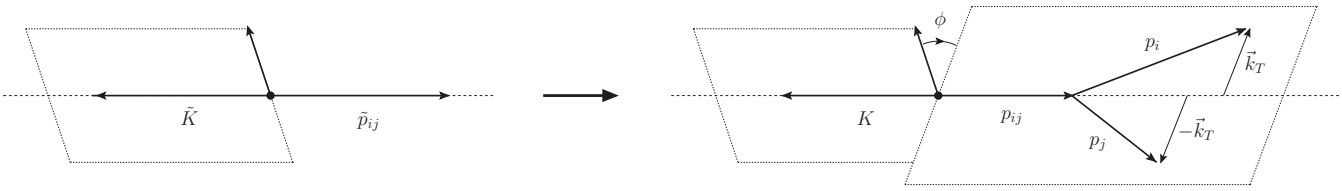

FIG. 2. Momentum assignment in splitting kinematics.

where the transverse momentum depends on the shifted momentum fractions

$$\tilde{z}_i^{(m)} = \tilde{z}_i + \frac{1}{2}\big(1 - v_{ij,k}\big)\,, \qquad \tilde{z}_j^{(m)} = \tilde{z}_j + \frac{1}{2}\big(1 - v_{ij,k}\big)\,, \qquad \text{with} \qquad v_{ij,k} = \sqrt{1 - \frac{p_{ij}^2 K^2}{Q^4}}\,. \tag{17}$$

In terms of the variable $y_{ij,K} = (p_i p_j)/(p_i p_j + p_{ij} K)$, the boundaries $z_\pm$ for the integration of the light-cone momentum fractions are given by

$$z_\pm = \frac{1}{2} \pm \frac{\sqrt{\big[(1-y_{ij,K})(1-\hat{\kappa}) + 2\hat{\kappa}\big]^2 - 4\hat{\kappa}}}{2(1-y_{ij,K})(1-\hat{\kappa})}\,, \tag{18}$$

and we obtain the spin-averaged forms of the pure splitting remainder functions

$$\begin{aligned}
\langle V_{gq,k}^{\rm coll}\rangle &= 8\pi\mu^{2\varepsilon}\alpha_s\, C_F\,(1-\varepsilon)\,\tilde{z}_j\,,\\
\langle V_{q\bar{q},k}^{\rm coll}\rangle &= 8\pi\mu^{2\varepsilon}\alpha_s\, C_F\left\{1 - \frac{2}{1-\varepsilon}\Big[\,\tilde{z}_i\tilde{z}_j - (1-\eta)z_+z_-\Big]\right\},\\
\langle V_{gg,k}^{\rm coll}\rangle &= 16\pi\mu^{2\varepsilon}\alpha_s\, C_A\left\{\tilde{z}_i\tilde{z}_j - (1-\eta)z_+z_-\right\}.
\end{aligned} \tag{19}$$

The pure splitting integrated counter-term is given by

$$\begin{aligned}
\frac{\alpha_s}{2\pi}\frac{1}{\Gamma(1-\varepsilon)}\left(\frac{4\pi\mu^2}{s_{ik}}\right)^{\varepsilon} I_{ij}^{(\rm p)}(\hat{\kappa}) &\equiv \int {\rm d}\Phi_{+1}(q;\tilde{p}_{ij},\tilde{K};p_i,p_j)\frac{1}{2p_ip_j}\langle V_{ij,k}\rangle\\
&= \frac{\alpha_s}{2\pi}\left(\frac{\mu^2}{Q^2}\right)^{\varepsilon}\frac{\Omega(3-2\varepsilon)}{(4\pi)^{1-2\varepsilon}}\,(1-\hat{\kappa})^{1-3\varepsilon}\int {\rm d}y\, y^{-1-\varepsilon}\,(1-y)^{1-2\varepsilon}\,\big(z_+ - z_-\big)^{1-2\varepsilon}\,\bar{\gamma}_{ab}(\varepsilon)\,,
\end{aligned} \tag{20}$$

where $y = y_{ij,K}$, and where

$$\bar{\gamma}_{ab}(\varepsilon) = \frac{\Omega(2-2\varepsilon)}{\Omega(3-2\varepsilon)}\Big(\frac{z_+ - z_-}{2}\Big)^{-1+2\varepsilon}\int_{z_-}^{z_+}{\rm d}z\,\big((z-z_-)(z_+-z)\big)^{-\varepsilon}\,\frac{\langle V_{ij,k}\rangle}{8\pi\alpha_s\mu^{2\varepsilon}}\,. \tag{21}$$

We use the techniques in [48, 81] to compute the integrals as a power series in ε. In particular,

$$\begin{aligned}
\frac{\alpha_s}{2\pi}\frac{1}{\Gamma(1-\varepsilon)}\left(\frac{4\pi\mu^2}{s_{ik}}\right)^{\varepsilon} I_{ij}^{(p)}(\hat{\kappa}) = \frac{\alpha_s}{2\pi}\left(\frac{\mu^2}{Q^2}\right)^{\varepsilon}\frac{(4\pi)^\varepsilon}{\Gamma(1-\varepsilon)}\int {\rm d}y\,\left\{-\frac{\delta(y)}{\varepsilon}\left(\frac{1-\sqrt{\hat{\kappa}}}{1+\sqrt{\hat{\kappa}}}\right)^{-\varepsilon} + \frac{1}{[y]_+}\right\}\\
\times\,\frac{\big(\big[(1-y)(1-\hat{\kappa})+2\hat{\kappa}\big]^2 - 4\hat{\kappa}\big)^{1/2-\varepsilon}}{(1-\hat{\kappa})^{1-\varepsilon}}\,\frac{\Gamma(1-\varepsilon)^2}{\Gamma(2-2\varepsilon)}\,\bar{\gamma}_{ab}(\varepsilon)\,.
\end{aligned} \tag{22}$$

Performing the y-integration and expanding the result up to $\mathcal{O}(\varepsilon^0)$ yields

$$
\begin{aligned}
I_{qq}^{(p)}(\hat{\kappa}) =& -\frac{1}{2\varepsilon} - \frac{1}{2}\log\frac{s_{ik}}{Q^2} - 1 + \log(1-\hat{\kappa}) + \frac{1}{2}\frac{\hat{\kappa}\log\hat{\kappa}}{1-\hat{\kappa}}\,, \\
I_{gg}^{(p)}(\hat{\kappa}) =& -\frac{1}{6\varepsilon} - \frac{1}{6}\log\frac{s_{ik}}{Q^2} - \frac{4-\hat{\kappa}}{9(1-\hat{\kappa})} - \frac{\hat{\kappa}^{3/2}}{3}\frac{\arcsin\sqrt{\hat{\kappa}}-\pi/2}{(1-\hat{\kappa})^{3/2}} + \frac{1}{3}\log(1-\hat{\kappa}) \\
& - \frac{\hat{\kappa}(1-\eta)}{1-\hat{\kappa}}\left(\sqrt{\frac{\hat{\kappa}}{1-\hat{\kappa}}}\arctan\sqrt{\frac{1-\hat{\kappa}}{\hat{\kappa}}} - \frac{\log\hat{\kappa}}{2} - 1\right), \\
I_{gq}^{(p)}(\hat{\kappa}) =& -\frac{2}{3\varepsilon} - \frac{2}{3}\log\frac{s_{ik}}{Q^2} - \frac{16-22\hat{\kappa}}{9(1-\hat{\kappa})} + \frac{2\hat{\kappa}^{3/2}}{3}\frac{\arcsin\sqrt{\hat{\kappa}}-\pi/2}{(1-\hat{\kappa})^{3/2}} + \frac{4}{3}\log(1-\hat{\kappa}) + \frac{\hat{\kappa}\log\hat{\kappa}}{1-\hat{\kappa}} \\
& + \frac{4}{3}\frac{\hat{\kappa}(1-\eta)}{1-\hat{\kappa}}\left(\sqrt{\frac{\hat{\kappa}}{1-\hat{\kappa}}}\arctan\sqrt{\frac{1-\hat{\kappa}}{\hat{\kappa}}} - \frac{\log\hat{\kappa}}{2} - 1\right).
\end{aligned}
\tag{23}
$$

Note that these results differ from the ones presented in [81] due to a different definition of the splitting functions. Contrary to the collinear components of Eqs. (5.16)-(5.20) in [81], our collinear dipole functions in Eq. (16) do not include the velocity factor $1/v_{ij,k}$. The results discussed in Ref. [48] are obtained from the slightly more general form presented here by setting $\eta = 1$.

III. NUMERICAL TESTS AND VALIDATION

To validate the implementation of results of the previous section within the SHERPA event generator we proceed in three steps: first, we check the subtraction in representative processes to isolate and test individual insertion operators. Second, we compute integrated cross-section for various processes to ensure the correctness of the integrated counterterms. And third, the self-consistency of the implementation is checked by comparing the matched NLO results with pure parton-shower and the stability of the multi-jet merging for different merging cuts. Throughout, we benchmark our results against established Catani-Seymour (CS) subtraction implementation within SHERPA [87], thereby guaranteeing consistent parameter settings and application of phase space cuts.

For each process considered in the first step, we generate phase space points which, for a given set of emitter, emitted particle and spectator, are rescaled into the soft and collinear limits, using the procedure outlined in Ref. [88]. For these points we then evaluate the relative difference between the real-emission correction and the infrared counterterms in the CS and ALARIC subtraction scheme. This allows us to judge the quality of the approximations in the logarithmically enhanced regions. We present the results as box-and-whisker plots, with the boxes signifying the second and third quartile, and the median indicated as a line inside the box. The whiskers indicate the 5th and 95th percentile.

Starting with the simplest cases, we show in Fig. 3 the scaling for $e^+e^- \to q\bar{q}g$ (left) and $e^+e^- \to q\bar{q}q'\bar{q}'$ (right), testing the gluon emission and the gluon-to-quark splittings, respectively. Comparing CS and ALARIC subtraction we observe similar performances in the deep infrared region, with both CS and ALARIC subtraction tending to zero as expected. In the collinear limit, the ALARIC subtraction exhibits a slightly larger spread in the distribution than the CS subtraction, whereas the opposite is true in the soft limit. For all practical purposes, these differences can be disregarded.

Analogously, we examine the gluon-to-gluon and the quark-to-quark splittings using the $e^+e^- \to q\bar{q}ggg$ (left) and $e^+e^- \to q\bar{q}q'\bar{q}'g$ (right) processes, respectively. The results are shown in Fig. 4. Again we find similar scaling behavior for both subtraction schemes.

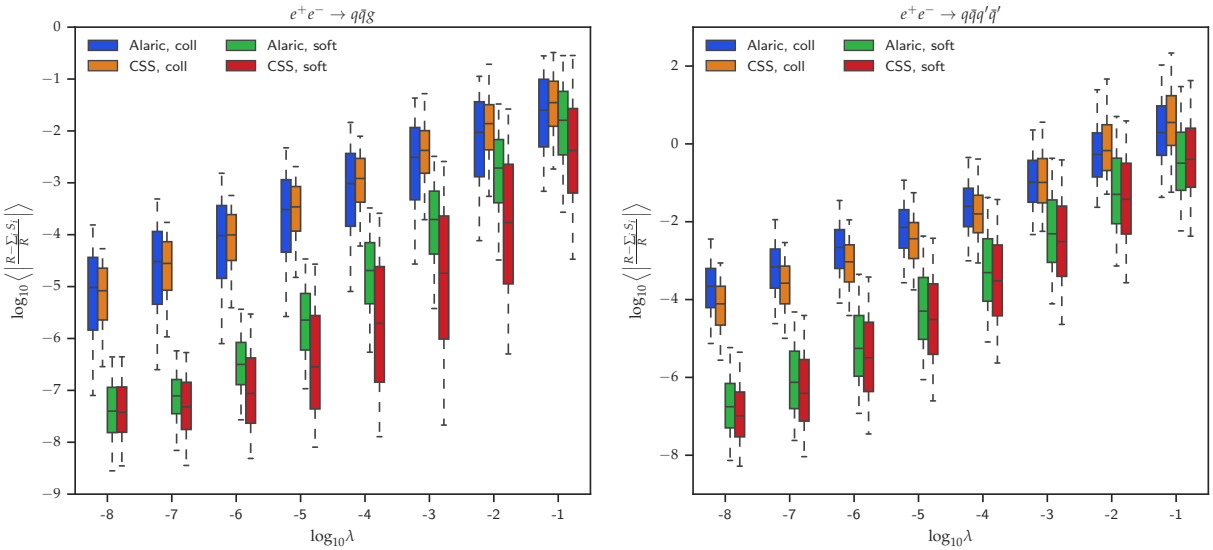

FIG. 3. Left: Scaling of CS and Alaric subtraction for $ee \to q\bar{q}g$ with $i = g$, $j = d$ and $k = \bar{d}$. Right: Scaling of CS and Alaric subtraction for $ee \to q\bar{q}q'\bar{q}'$ with $i = d$, $j = \bar{d}$ and $k = u$.

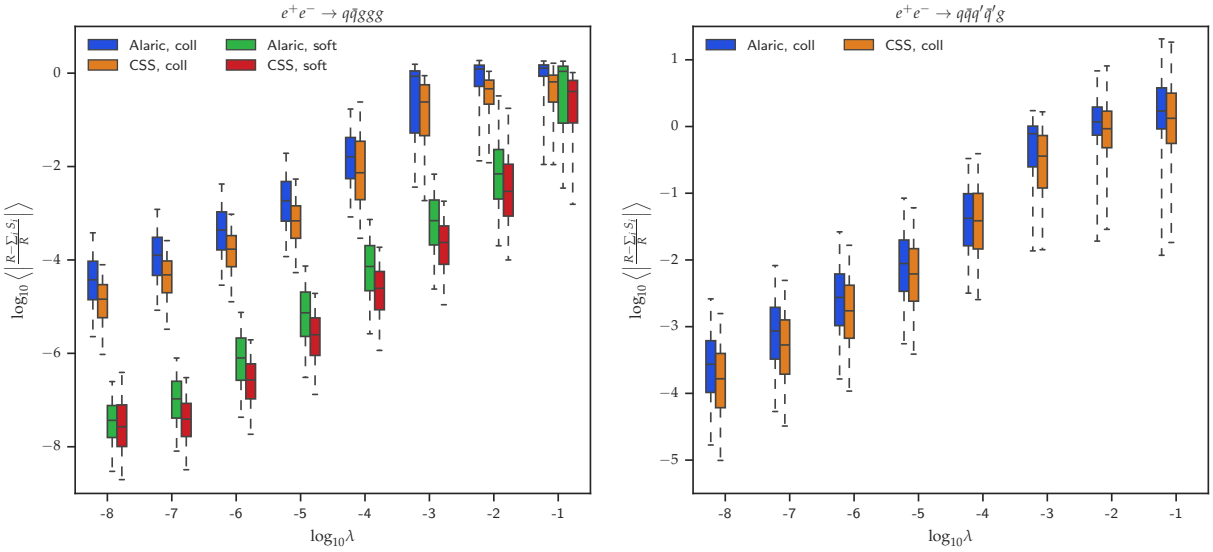

FIG. 4. Left: Scaling of CS and Alaric subtraction for $ee \to q\bar{q}ggg$ with $i = g$, $j = g$ and $k = g$. Right: Scaling of CS and Alaric subtraction for $ee \to q\bar{q}q'\bar{q}'g$ with $i = u$, $j = \bar{u}$ and $k = \bar{d}$.

We validate the implementation of the integrated counter-terms by comparing inclusive cross sections. For clarity, we only present numbers relevant for an informed comparison, i.e., the integrated counter-terms and the real-subtracted cross-section for each subtraction scheme. In the trivial case of $e^+e^- \to 2$ jets at $\sqrt{s} = 91.2$ GeV, shown in Tab. I, we find excellent agreement, with about 0.8σ difference in total cross section between the CS and ALARIC schemes. In this case the integrated counter term for the soft emission actually reduces to the exact same expression in both cases, cf. the discussion in Sec. II A. In order to verify the subtraction scheme for a non-trivial recoil dependence, we investigate the cross section for $e^+e^- \to ZH$ with a stable Z boson and the Higgs boson decaying into gluons at a hypothetical FCC-ee at $\sqrt{s} = 240$ GeV. Table I shows excellent agreement between the two schemes, with a remaining difference of about 0.7σ.

Turning to more complicated processes, we compute total cross sections for $e^+e^- \to 3$ jets, $e^+e^- \to 4$ jets and $e^+e^- \to 5$ jets, all at $\sqrt{s} = 91.2$ GeV. The results are presented in Tab. II. The errors of the individual cross sections stay below the permille level, and we find agreement between the schemes at the level of about 1σ for 3-jet production.

$e^+e^- \to 2$ jets $\sqrt{s} = 91.2$ GeV, $\mu_R = \sqrt{s}$	I [pb]	ΔI [pb]	RS [pb]	ΔRS [pb]	IRS [pb]	ΔIRS [pb]	ΔIRS/NLO
CS	131.9	<0.01	-505.79	0.19	-373.89	0.19	0.004‰
ALARIC	131.9	<0.01	-505.61	0.12	-373.71	0.12	0.003‰
CS-ALARIC					-0.18 ± 0.22		

$e^+e^- \to ZH[\to gg]$ $\sqrt{s} = 240$ GeV, $\mu_R = M_H$	I [pb]	ΔI [pb]	RS [pb]	ΔRS [pb]	IRS [pb]	ΔIRS [pb]	ΔIRS/NLO
CS	$-8.4 \cdot 10^{-4}$	$0.03 \cdot 10^{-5}$	$6.31 \cdot 10^{-5}$	$0.07 \cdot 10^{-5}$	$-7.8 \cdot 10^{-4}$	$0.08 \cdot 10^{-5}$	0.1‰
ALARIC	$-8.4 \cdot 10^{-4}$	$0.03 \cdot 10^{-5}$	$6.36 \cdot 10^{-5}$	$0.07 \cdot 10^{-5}$	$-7.8 \cdot 10^{-4}$	$0.08 \cdot 10^{-5}$	0.1‰
CS-ALARIC					$(0.005 \pm 0.011) \cdot 10^{-4}$		

TABLE I. Subtraction-scheme dependent cross-section contributions for $e^+e^- \to 2$ jets and for $e^+e^- \to ZH$ with the Higgs boson decaying into gluons. In both cases the complete hadronic final state defines the recoil system.

$e^+e^- \to n$ jets @ 91.2 GeV $\mu_R = \sqrt{s}$, $y_{n,n-1} > (10\,\text{GeV})^2/s$		I [pb]	ΔI [pb]	RS [pb]	ΔRS [pb]	IRS [pb]	ΔIRS [pb]	ΔIRS/NLO
n=3	CS	5118.85	0.37	-1034.4	1.4	4084.45	1.4	0.1‰
	ALARIC	5174.47	0.38	-1087.6	1.8	4086.84	1.8	0.1‰
	CS-ALARIC					-2.39 ± 2.32		
n=4	CS	938.97	0.12	-94.45	0.73	844.52	0.74	0.5‰
	ALARIC	922.36	0.12	-79.75	0.70	842.61	0.71	0.5‰
	CS-ALARIC					1.91 ± 1.03		
n=5	CS	46.1544	0.015	-2.341	0.058	43.813	0.060	1‰
	ALARIC	44.6125	0.014	-0.857	0.067	43.756	0.068	1‰
	CS-ALARIC					0.057 ± 0.091		

TABLE II. Subtraction-scheme dependent cross-section contributions for $e^+e^- \to nj$. The center-of-mass energy is set to $\sqrt{s} = 91.2$ GeV. Jets are defined according to the Durham algorithm [89] and are required to satisfy a cut on the jet resolution from n to $n-1$ jets, $y_{n,n-1}$.

In the 4-jet case, the two results agree at the level of 1.85σ. For the production of 5 jets, we observe agreement at around 0.6σ. These results confirm the robustness and consistency of the ALARIC subtraction scheme up to high jet multiplicities.

In order to validate our implementation of the MC@NLO technology, we compare the differential jet rates in the Durham algorithm between parton-shower predictions and matched results. Figure 5 displays the $2 \to 3$-jet rate (left) and the $3 \to 4$-jet rate (right) as predicted by a simulation from the pure ALARIC parton shower, and from the next-to-leading order matched ALARIC simulation. The increase in the total rate of the process by the expected K-factor of α_s/π is clearly visible. In addition, we observe that the scale uncertainty in this simulation is not reduced, because the real radiative corrections that determine the jet rates are predicted (mostly) by the parton shower in both cases. They are therefore endowed with variations determined by Eq. (25), cf. the discussion in Sec. IV.

Next we investigate the stability of the multi-jet merging. In Fig. 6 we show the $2 \to 3$ and $3 \to 4$ jet rate in the Durham k_T-algorithm [89] for different values of the merging cut, Q_{cut}. The Q_{cut} values are indicated in the figure by vertical lines and are varied over a relatively large range. The colored histograms indicate the contributions to the multi-jet merged result from sub-samples with 2-jet through 5-jet fixed-order calculations. For the $2 \to 3$ jet rate, we expect a transition from the 2-jet sub-sample to 3-jet and higher multiplicity sub-samples at the merging cut. For the $3 \to 4$ jet rate, we expect a transition from the 2-jet and 3-jet sub-samples below the merging cut, to 4-jet and higher multiplicity matrix elements above the merging cut. We find that the variation of the overall distribution (in black) around the merging cuts is of less than 10%, and in most cases even smaller. This indicates a good approximation of the matrix element by the parton shower, even at relatively high resolution scale.

Finally, we illustrate the flexibility in choosing the recoil system by calculating matched predictions for Higgs boson decays to gluons in the Higgstrahlung production mode $e^+e^- \to ZH$, where we choose the Higgs as the recoil system. Event shapes in this final state have in the past been computed with quark-gluon discrimination at a potential future lepton collider like the FCC in mind [90–96]. We correspondingly choose a center of mass energy of $\sqrt{s} = 240$ GeV

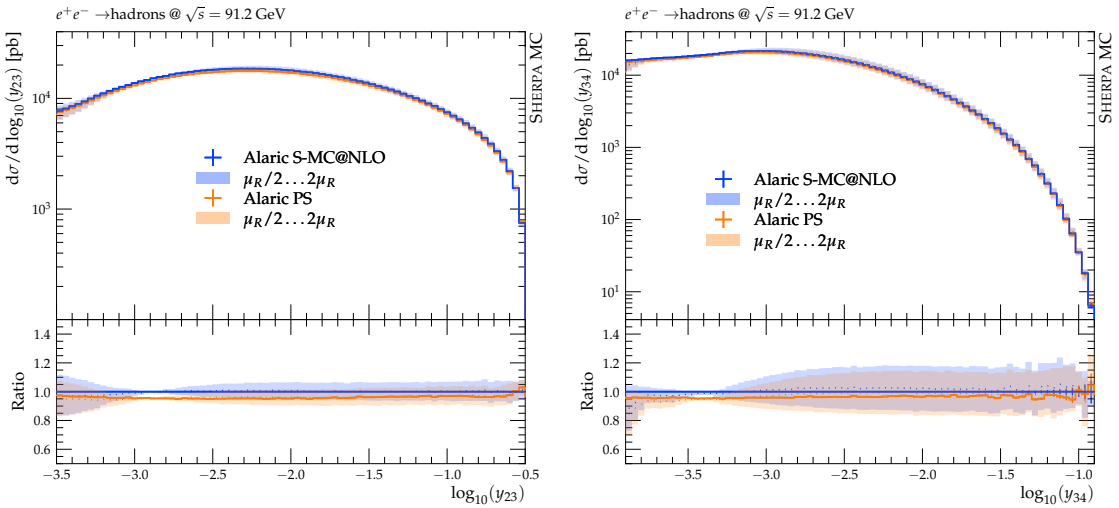

FIG. 5. Comparison of S-MC@NLO and pure parton-shower predictions for the differential $2 \to 3$- and $3 \to 4$-jet rates in the Durham algorithm at parton level. See the main text for details.

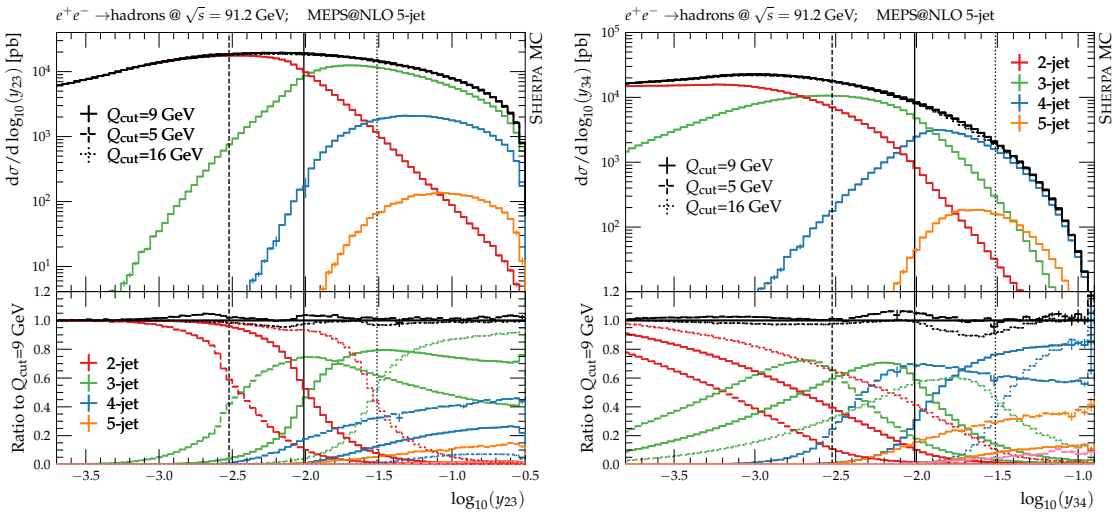

FIG. 6. Q_{cut} dependence of the differential $2 \to 3$- and $3 \to 4$-jet rates in the Durham algorithm at parton level. See the main text for details.

[9]. As renormalisation scale we use the Higgs mass M_H. In Fig. 7 we show the normalized distributions for the Durham jet rate y_{23} (left) and thrust τ (right), calculated in the center of mass frame of the Higgs decay products, at MC@NLO accuracy. We observe mild effects, at most of order 10%, in the region of large observable values where fixed order corrections are expected to be important. In the soft regions we observe no effects on the central values, but a significant reduction in scale uncertainty, which is a consequence of the changes in the hard region by means of parton-shower unitarity.

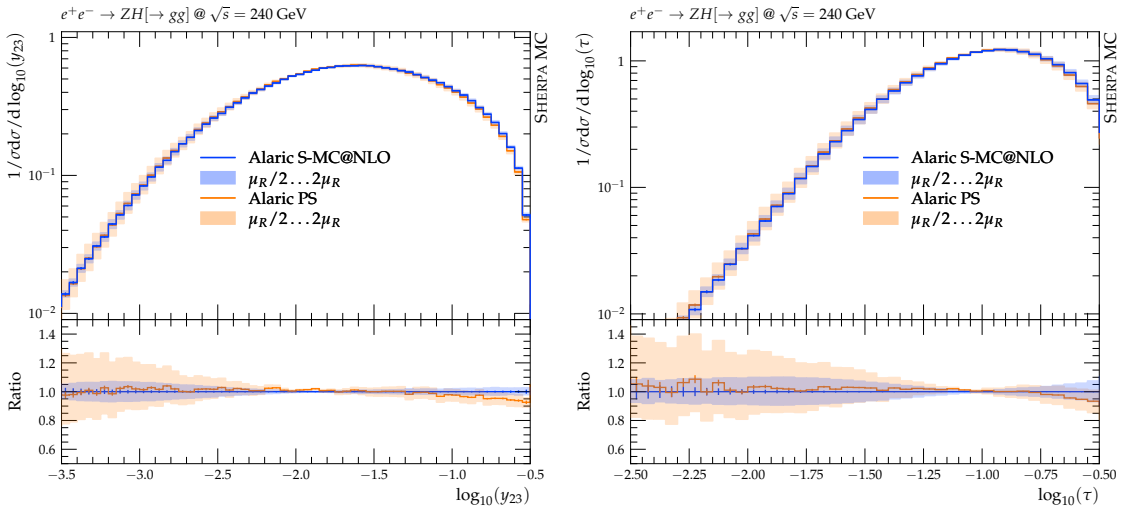

FIG. 7. Comparison of S-MC@NLO and pure parton-shower predictions for the differential $2 \to 3$ jet rate in the Durham algorithm and the thrust observable in $e^+e^- \to ZH[\to gg]$.

IV. PHENOMENOLOGY

This section contains the first numerical results obtained with the matching and merging techniques for the ALARIC parton shower. We rely on the event generation framework SHERPA [97–100] for the computation of the hard cross section [101, 102], the implementation of the generic components of the dipole subtraction [87], and the interface with the one-loop providers, in this case MCFM [103–107] and OpenLoops [108–110]. We use the color-correct S-MC@NLO matching method, which accounts for non-trivial spin correlations across the hard process and the first splitting [61, 83]. We set $C_F = (N_c^2 - 1)/(2N_c) = 4/3$ and $C_A = 3$, and all quarks are considered to be massless. However, we implement heavy-flavor thresholds at $m_c = 1.42$ GeV and $m_b = 4.92$ GeV. The running coupling is evaluated at two-loop accuracy with $\alpha_s(m_z) = 0.118$. Following standard practice to improve the logarithmic accuracy of the parton shower, we include the effect of the two-loop cusp anomalous dimension through a rescaling of the scalar part of the splitting function [111]. All analyses are performed with RIVET [112–114].

We adopt a scale variation scheme that reflects the NLL-correct momentum mapping in the Alaric parton shower. We first note that most parton showers use a renormalization scale based on the transverse momentum of the emission, which captures the effects of those higher-order corrections that are due to phase-space restrictions of real corrections in subsequent radiation [115]. While the precise definition of the transverse momentum is unambiguous in Ref. [115], there is considerable freedom to vary its functional form if no more than NLL precision is to be achieved. This freedom is explored in existing parton shower models. It is also known that the finite part of higher-order corrections to soft gluon emission, which stem from the collinear decay of the gluon, contribute a K-factor proportional to the two-loop cusp anomalous dimension [116–119] that can be absorbed into the renormalization scale [111]. This factor is of the form

$$K(t) = \left(\frac{67}{18} - \frac{\pi^2}{6}\right) C_A - \frac{10}{9} T_R\, n_f(t)\,, \tag{24}$$

where $n_f(t)$ is the number of active flavors at scale t and t itself is of transverse momentum type. To be consistent with all leading higher-order effects at NLL precision, the scalar splitting functions in ALARIC must thus take the form

$$V_{ij,k}^{(s)}\left[1 + \frac{\alpha_s(t)}{2\pi}\left(\beta_0(t)\log\frac{k_T^2}{t} + K(t)\right)\right], \tag{25}$$

where $\beta_0(t) = 11/3\,C_A - 4/3\,T_R\,n_f(t)$. When performing a leading-order multi-jet merging with ALARIC, the renormalization scales to be used in the hard matrix elements are determined by this constraint. This is a consequence of the required consistency between the parton-shower evolution and the fixed-order calculation: to guarantee correct merging, the latter needs to only contribute finite corrections, but must not include logarithmic enhancements. When performing a next-to-leading order merging, the $\mathcal{O}(\alpha_s)$ corrections are fully incorporated by the fixed-order

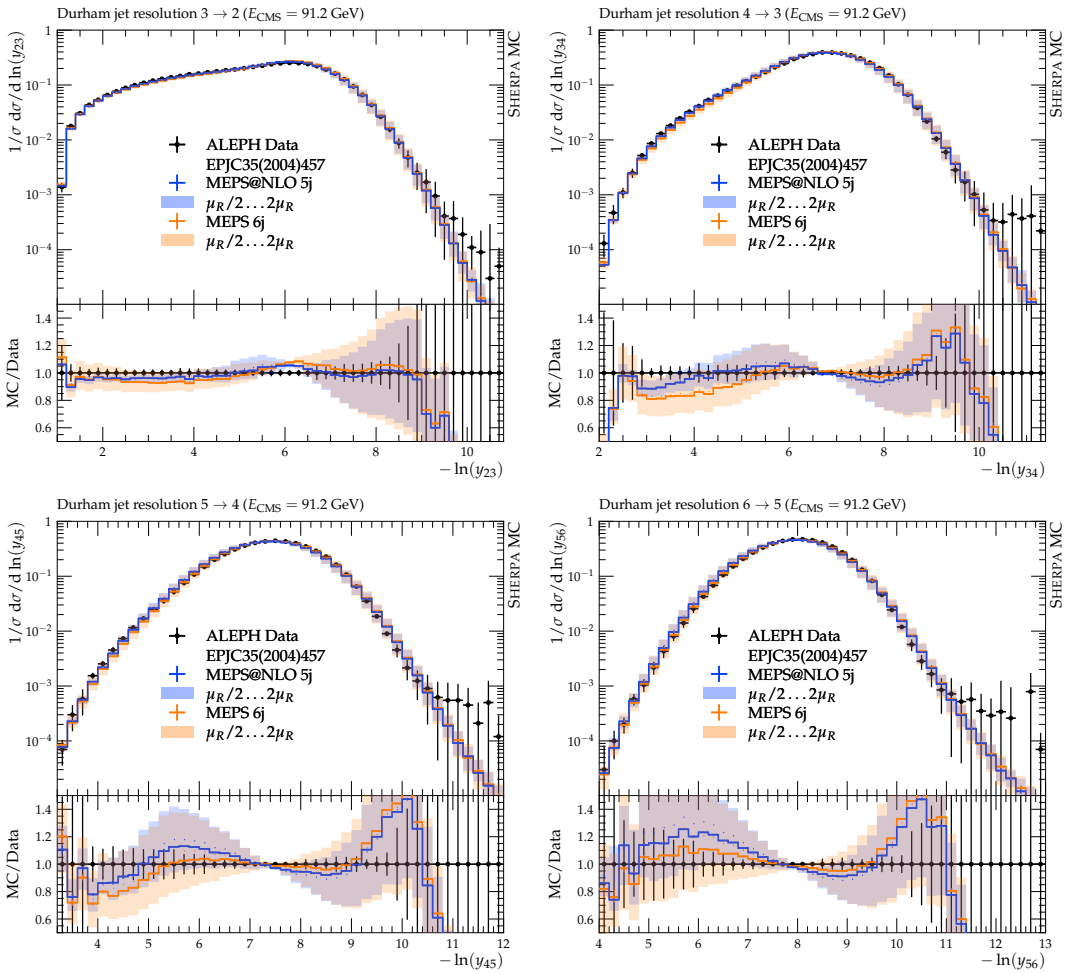

FIG. 8. Perturbative uncertainties in MEPS and MEPS@NLO predictions of differential jet rates compared to data from ALEPH [120].

calculation. To prevent double counting, they must thus not be included in the renormalization scale setting. When performing scale variations in the following, we account for the above constraints and begin with a variation of the renormalization scale in the parton shower. The renormalization scale in the fixed-order calculation is then chosen accordingly.

We first discuss differential jet rates in the Durham jet algorithm [89]. Measurements of these quantities have been performed by the ALEPH collaboration [120] and by the JADE and OPAL collaborations [121]. The ALARIC simulations include up to six jets from hard matrix elements at the leading order, and up to five jets from hard matrix elements at the next-to-leading order, with the merging cut set to 7 GeV. The corresponding predictions from ALARIC in comparison to the experimental measurements are shown in Figs. 8 and 9. We observe excellent agreement of the multi-jet merged results with both experimental measurements, both at leading, and at next-to-leading order. It is worth noting that the systematic uncertainties from scale variations in the hard, perturbative region of y_{23} are much smaller in the case of NLO merging than they are in the case of leading-order merging. This is due to the fact that the hard region of this observable is described mostly at NLO precision by the 3-, 4- and 5-jet fixed-order contributions to the merging, while yet higher multiplicity contributions are very small due to restricted phase space. For y_{34} there is still a considerable improvement, but it is not as pronounced as in the case of y_{23}, because there is significant phase space for 6-parton fixed-order contributions which are described at leading order precision in our setup. For y_{45} and y_{56} the improvement from the NLO merging is diminishing, consistent with the fact that the 6-parton matrix elements are pure leading order, and thus inherit the relatively large renormalization scale dependence from the parton shower.

Figure 10 shows the thrust [123] distribution as measured by the ALEPH collaboration [120] (left), and the moments of thrust as measured by the OPAL collaboration [122] (right). The thrust observable is known to very high accuracy

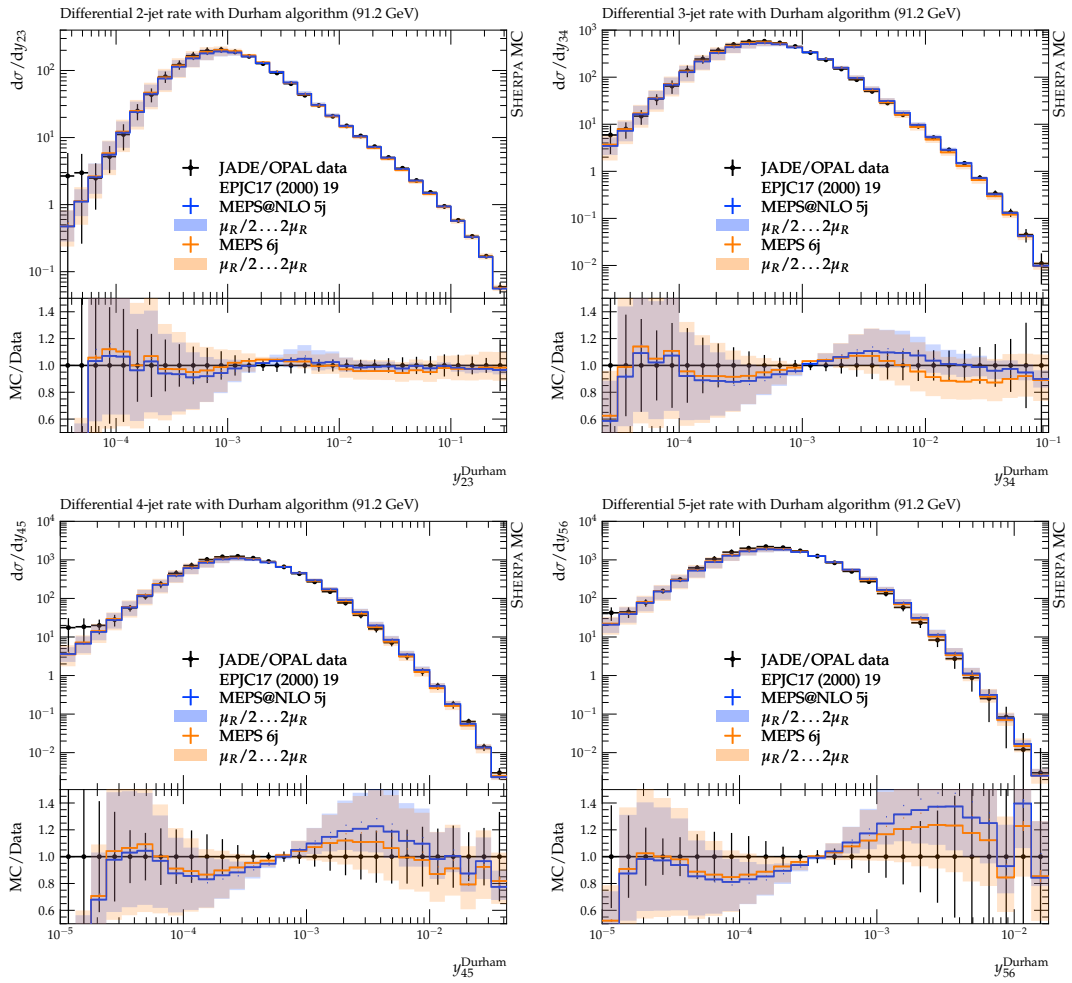

FIG. 9. Perturbative uncertainties in MEPS and MEPS@NLO predictions of differential jet rates compared to data from JADE & OPAL [121].

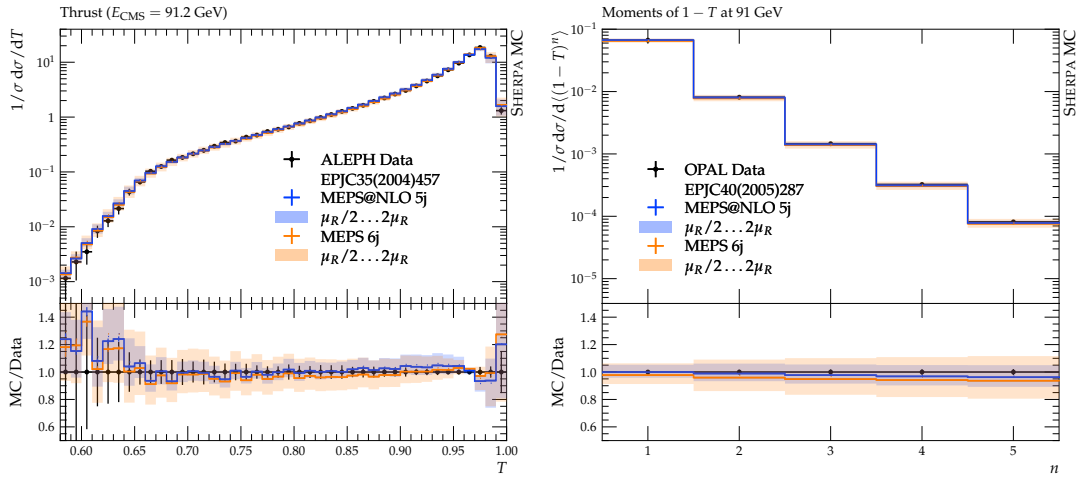

FIG. 10. Perturbative uncertainties in MEPS and MEPS@NLO predictions of thrust. Compared are the measurements for the event shape from ALEPH [120] and its moments from OPAL [122].

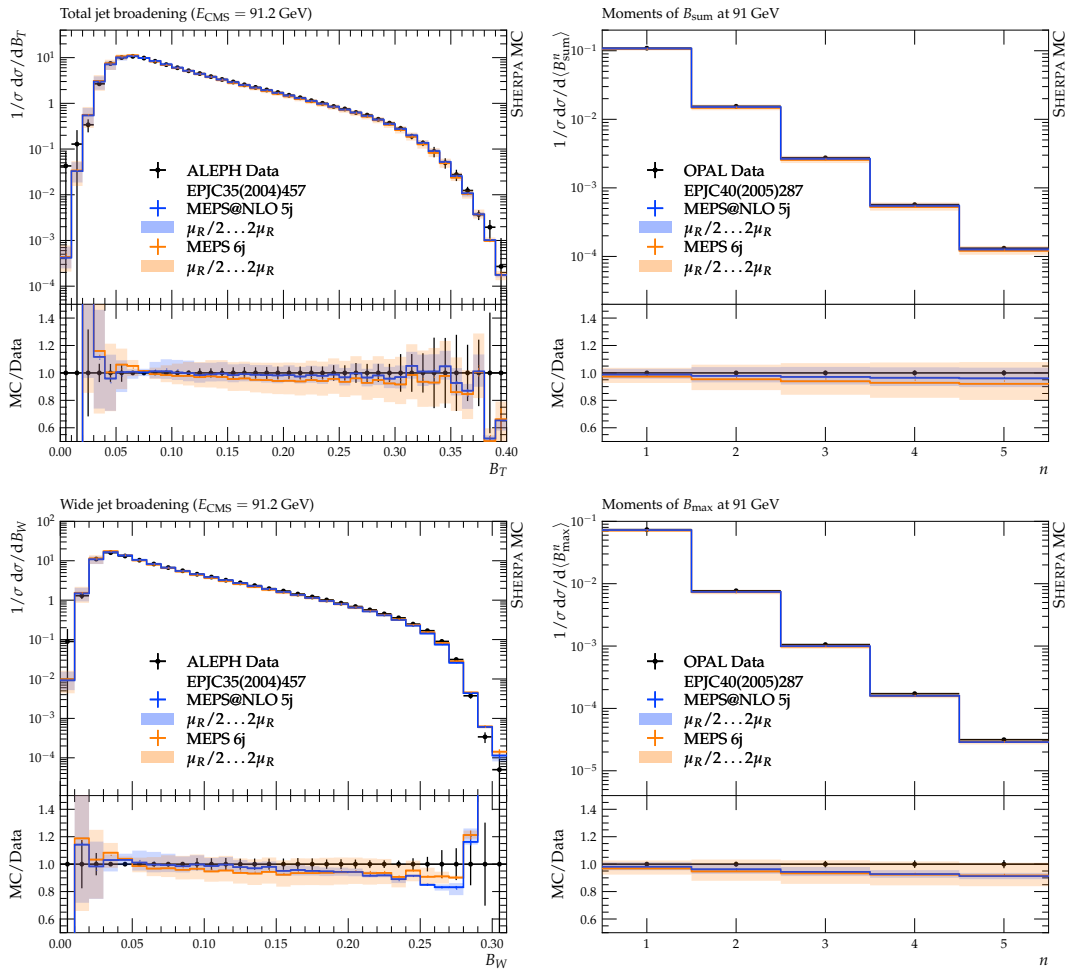

FIG. 11. Perturbative uncertainties in MEPS and MEPS@NLO predictions of total jet/hemisphere broadening (top) and wide jet/hemisphere broadening (bottom). Compared are the measurements from ALEPH [120] and OPAL [122].

in (resummed) perturbation theory. Due to the intricate structure of non-perturbative corrections [124], a coherent description at the hadron level has, however, only been achieved recently. Our prediction consistently includes the differences in power corrections that occur in the different regions, and it naturally extends beyond the Sudakov shoulder [125] due to the complete phase-space coverage in the multi-jet calculations. It is therefore not unexpected that the predictions give excellent agreement with the experimental data. We observe a reduction of the perturbative uncertainty by about a factor two in the bulk of the phase space, and a smaller reduction in the region beyond the Sudakov shoulder. This is in line with the effects discussed for the Durham jet rates.

The top panels of Fig. 11 show the total jet broadening distribution as measured by the ALEPH collaboration [120] (left), and the moments of total broadening as measured by the OPAL collaboration [122] (right). Again, we observe a significantly improved description of the experimental data with NLO merged predictions, and a reduction of perturbative uncertainties by about a factor of two. Similar improvements are found for wide jet broadening and its moments, shown in Fig. 11 (bottom).

Figure 12 shows the distribution of the C-parameter as measured by the ALEPH collaboration [120] (left), and the moments of the C-parameter as measured by the OPAL collaboration [122] (right). The description of the distribution is achieved with similar quality in the case of leading- and next-to-leading order merging; however, the moments show a clear preference for the next-to-leading order merged result. Again, the renormalization scale uncertainty is reduced by about a factor of two in both cases.

As the last event shape variable, we investigate sphericity. Figure 13 shows its distribution as measured by the ALEPH collaboration [120] (left), and its moments as measured by the OPAL collaboration [122] (right). We observe a significant improvement in the description of both the distribution and its moments in the next-to-leading order

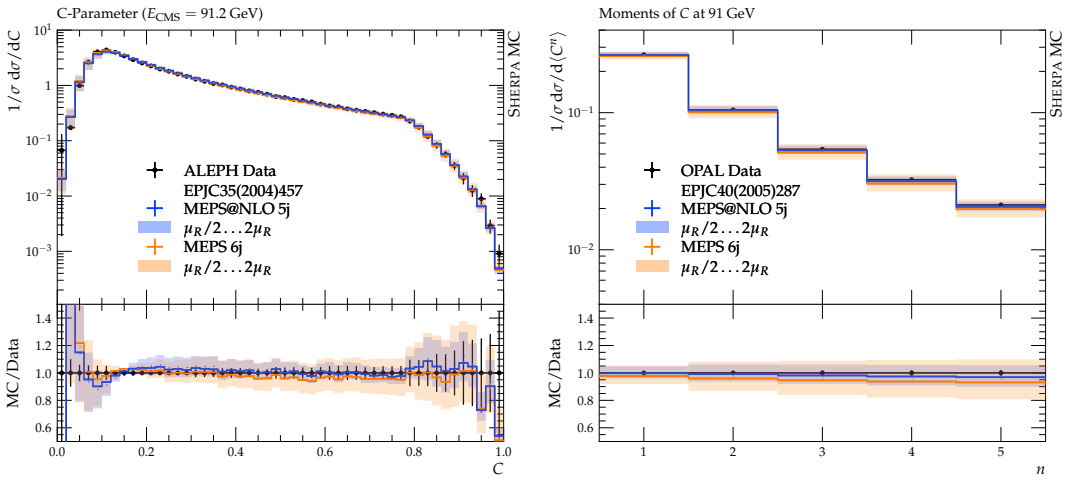

FIG. 12. Perturbative uncertainties in MEPS and MEPS @NLO predictions of the C-parameter. Compared are the measurements from ALEPH [120] and OPAL [122].

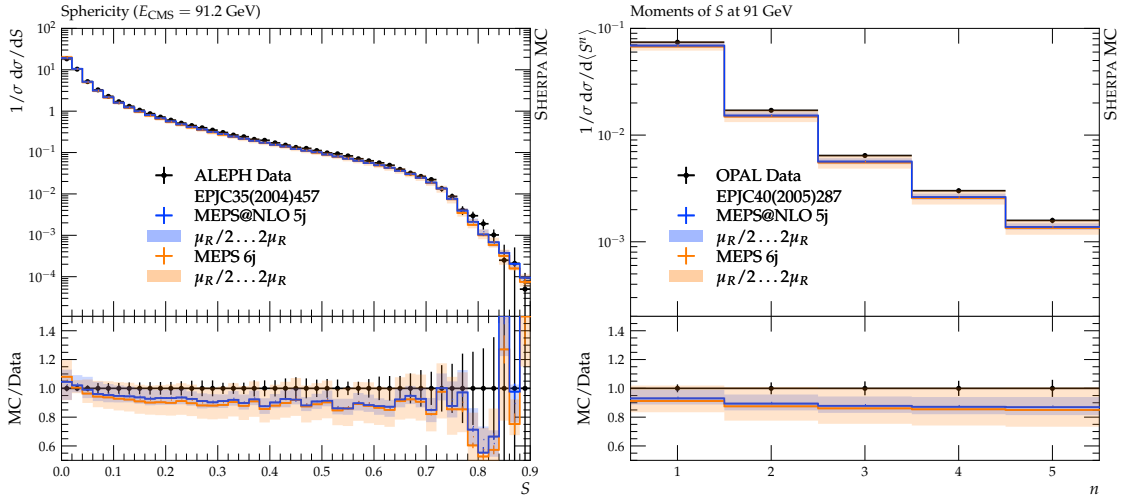

FIG. 13. Perturbative uncertainties in MEPS and MEPS@NLO predictions of sphericity. Compared are the measurements from ALEPH [120] and OPAL [122].

merged predictions. Again, the perturbative uncertainties are reduced to about half of their size at leading order.

Finally, we compare leading- and next-to-leading order merged predictions for the four-jet angles measured by the OPAL collaboration [126]. Figure 14 shows that no improvement is obtained in the simulation using next-to-leading order merging methods when compared to leading-order merging. It is difficult to judge the quality of the Monte-Carlo predictions due to the missing experimental uncertainties.

V. OUTLOOK

In this manuscript, we have derived various analytic expressions needed for a process-independent implementation of an infrared subtraction scheme based on the ALARIC parton shower model. We have validated the subtraction in the processes of $e^+e^- \to n$ jets, with n ranging from two to five, which is the current state of the art for high-multiplicity fixed-order multi-jet calculations at a lepton collider [127]. Making use of the fixed-order subtraction, we have developed the first S-MC@NLO matching method for the ALARIC parton shower, and applied it to the phenomenologically important reactions of e^+e^- →hadrons and gluonic decays of the Higgs boson. Utilizing the generic implementation

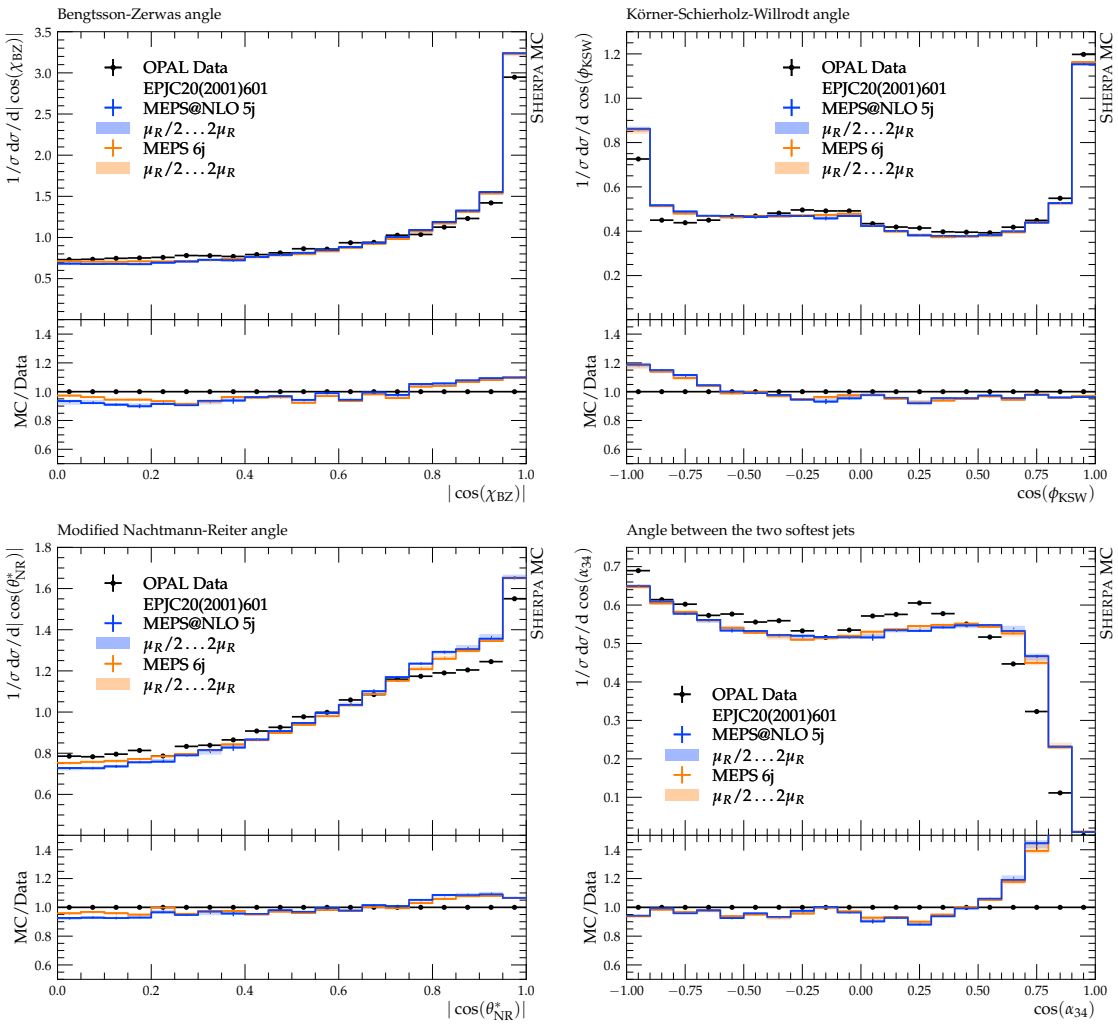

FIG. 14. Four-jet angles using the Durham algorithm compared to data from OPAL [126].

of next-to-leading order multi-jet merging methods in the SHERPA event generator, we combined the next-to-leading order matched predictions for 2-, 3-, 4- and 5-jets and presented the first multi-jet merged simulation for color singlet decays at the Z pole with a modern parton shower. The comparison to experimental data clearly demonstrates the improvements obtained with next-to-leading order multi-jet merging, and shows an encouraging reduction of the perturbative uncertainties that will be crucial in view of a potential future lepton collider such as the FCC-ee.

In the near future we will extend the NLO matching of the ALARIC parton-shower model to processes with colored particles in the initial state, and include the matching for final states with heavy quarks. In addition, we expect to include higher-order corrections to the evolution in the form of triple collinear and double soft contributions to the splitting functions, and more generally an extension towards higher logarithmic precision of the parton shower model. The current state of the art simulations will be made available in a next minor public version of the SHERPA event generator.

ACKNOWLEDGMENTS

This manuscript has been authored by Fermi Forward Discovery Group, LLC under Contract No. 89243024CSC000002 with the U.S. Department of Energy, Office of Science, Office of High Energy Physics. The work of S.H. was supported by the U.S. Department of Energy, Office of Science, Office of Advanced Scientific Computing Research, Scientific Discovery through Advanced Computing (SciDAC-5) program, grant "NeuCol". F.K. gratefully acknowledges support by STFC under grant agreement ST/P006744/1. P.M. is supported by the Swiss National Science Foundation (SNF)

under contract 200020-204200. D.R. is supported by the European Union under the HORIZON program in Marie Skłodowska-Curie project No. 101153541. During parts of this work, D.R. was further supported by STFC under grant agreement ST/P006744/1 as well as by the Durham University Physics Department Developing Talents Award and by the German Academic Exchange Service (DAAD).

[1] A. Buckley *et al.*, Phys. Rept. **504**, 145 (2011), arXiv:1101.2599 [hep-ph].
[2] J. M. Campbell *et al.*, SciPost Phys. **16**, 130 (2024), arXiv:2203.11110 [hep-ph].
[3] G. Aad *et al.* (ATLAS), JINST **3**, S08003 (2008).
[4] S. Chatrchyan *et al.* (CMS), JINST **3**, S08004 (2008).
[5] A. A. Alves, Jr. *et al.* (LHCb), JINST **3**, S08005 (2008).
[6] K. Aamodt *et al.* (ALICE), JINST **3**, S08002 (2008).
[7] M. Benedikt *et al.* (FCC), (2025), 10.17181/CERN.9DKX.TDH9, arXiv:2505.00272 [hep-ex].
[8] M. Benedikt *et al.* (FCC), (2025), 10.17181/CERN.EBAY.7W4X, arXiv:2505.00274 [physics.acc-ph].
[9] M. Benedikt *et al.* (FCC), (2025), 10.17181/CERN.I26X.V4VF, arXiv:2505.00273 [physics.acc-ph].
[10] B. R. Webber, Nucl. Phys. B **238**, 492 (1984).
[11] M. Bengtsson, T. Sjöstrand, and M. van Zijl, Z. Phys. C **32**, 67 (1986).
[12] M. Bengtsson and T. Sjöstrand, Nucl. Phys. B **289**, 810 (1987).
[13] G. Marchesini and B. R. Webber, Nucl. Phys. B **310**, 461 (1988).
[14] B. Andersson, G. Gustafson, and L. Lönnblad, Nucl. Phys. B **339**, 393 (1990).
[15] B. R. Webber, Ann. Rev. Nucl. Part. Sci. **36**, 253 (1986).
[16] M. Bengtsson and T. Sjöstrand, Phys. Lett. B **185**, 435 (1987).
[17] J. C. Collins, Nucl. Phys. B **304**, 794 (1988).
[18] I. G. Knowles, Nucl. Phys. B **304**, 767 (1988).
[19] I. G. Knowles, Nucl. Phys. B **310**, 571 (1988).
[20] I. G. Knowles, Comput. Phys. Commun. **58**, 271 (1990).
[21] M. van Beekveld, S. Ferrario Ravasio, K. Hamilton, G. P. Salam, A. Soto-Ontoso, G. Soyez, and R. Verheyen, JHEP **11**, 020 (2022), arXiv:2207.09467 [hep-ph].
[22] Z. Nagy and D. E. Soper, JHEP **10**, 024 (2005), arXiv:hep-ph/0503053.
[23] Z. Nagy and D. E. Soper, in *Ringberg Workshop on New Trends in HERA Physics 2005* (2006) pp. 101–123, arXiv:hep-ph/0601021.
[24] S. Schumann and F. Krauss, JHEP **03**, 038 (2008), arXiv:0709.1027 [hep-ph].
[25] W. T. Giele, D. A. Kosower, and P. Z. Skands, Phys. Rev. D **78**, 014026 (2008), arXiv:0707.3652 [hep-ph].
[26] S. Plätzer and S. Gieseke, JHEP **01**, 024 (2011), arXiv:0909.5593 [hep-ph].
[27] S. Höche and S. Prestel, Eur. Phys. J. C **75**, 461 (2015), arXiv:1506.05057 [hep-ph].
[28] N. Fischer, S. Prestel, M. Ritzmann, and P. Skands, Eur. Phys. J. C **76**, 589 (2016), arXiv:1605.06142 [hep-ph].
[29] B. Cabouat and T. Sjöstrand, Eur. Phys. J. C **78**, 226 (2018), arXiv:1710.00391 [hep-ph].
[30] Z. Nagy and D. E. Soper, JHEP **06**, 044 (2012), arXiv:1202.4496 [hep-ph].
[31] S. Plätzer and M. Sjödahl, JHEP **07**, 042 (2012), arXiv:1201.0260 [hep-ph].
[32] Z. Nagy and D. E. Soper, JHEP **06**, 097 (2014), arXiv:1401.6364 [hep-ph].
[33] Z. Nagy and D. E. Soper, JHEP **07**, 119 (2015), arXiv:1501.00778 [hep-ph].
[34] S. Plätzer, M. Sjödahl, and J. Thorén, JHEP **11**, 009 (2018), arXiv:1808.00332 [hep-ph].
[35] J. Isaacson and S. Prestel, Phys. Rev. D **99**, 014021 (2019), arXiv:1806.10102 [hep-ph].
[36] Z. Nagy and D. E. Soper, Phys. Rev. D **100**, 074005 (2019), arXiv:1908.11420 [hep-ph].
[37] Z. Nagy and D. E. Soper, Phys. Rev. D **99**, 054009 (2019), arXiv:1902.02105 [hep-ph].
[38] J. R. Forshaw, J. Holguin, and S. Plätzer, JHEP **08**, 145 (2019), arXiv:1905.08686 [hep-ph].
[39] S. Höche and D. Reichelt, Phys. Rev. D **104**, 034006 (2021), arXiv:2001.11492 [hep-ph].
[40] M. De Angelis, J. R. Forshaw, and S. Plätzer, Phys. Rev. Lett. **126**, 112001 (2021), arXiv:2007.09648 [hep-ph].
[41] J. Holguin, J. R. Forshaw, and S. Plätzer, Eur. Phys. J. C **81**, 364 (2021), arXiv:2011.15087 [hep-ph].
[42] G. Gustafson, Nucl. Phys. B **392**, 251 (1993).
[43] K. Hamilton, R. Medves, G. P. Salam, L. Scyboz, and G. Soyez, JHEP **03**, 041 (2021), arXiv:2011.10054 [hep-ph].
[44] M. Dasgupta, F. A. Dreyer, K. Hamilton, P. F. Monni, and G. P. Salam, JHEP **09**, 033 (2018), [Erratum: JHEP 03, 083 (2020)], arXiv:1805.09327 [hep-ph].
[45] M. Dasgupta, F. A. Dreyer, K. Hamilton, P. F. Monni, G. P. Salam, and G. Soyez, Phys. Rev. Lett. **125**, 052002 (2020), arXiv:2002.11114 [hep-ph].
[46] K. Hamilton, A. Karlberg, G. P. Salam, L. Scyboz, and R. Verheyen, JHEP **03**, 193 (2022), arXiv:2111.01161 [hep-ph].
[47] F. Herren, S. Höche, F. Krauss, D. Reichelt, and M. Schönherr, JHEP **10**, 091 (2023), arXiv:2208.06057 [hep-ph].
[48] B. Assi and S. Höche, Phys. Rev. D **109**, 114008 (2024), arXiv:2307.00728 [hep-ph].
[49] S. Höche, F. Krauss, and D. Reichelt, Phys. Rev. D **111**, 094032 (2025), arXiv:2404.14360 [hep-ph].
[50] C. T. Preuss, JHEP **07**, 161 (2024), arXiv:2403.19452 [hep-ph].
[51] S. Höche and S. Prestel, Phys. Rev. D **96**, 074017 (2017), arXiv:1705.00742 [hep-ph].

[52] F. Dulat, S. Höche, and S. Prestel, Phys. Rev. D **98**, 074013 (2018), arXiv:1805.03757 [hep-ph].
[53] L. Gellersen, S. Höche, and S. Prestel, Phys. Rev. D **105**, 114012 (2022), arXiv:2110.05964 [hep-ph].
[54] S. Ferrario Ravasio, K. Hamilton, A. Karlberg, G. P. Salam, L. Scyboz, and G. Soyez, Phys. Rev. Lett. **131**, 161906 (2023), arXiv:2307.11142 [hep-ph].
[55] M. van Beekveld, M. Dasgupta, B. K. El-Menoufi, J. Helliwell, P. F. Monni, and G. P. Salam, JHEP **03**, 209 (2025), arXiv:2409.08316 [hep-ph].
[56] S. Frixione and B. R. Webber, JHEP **06**, 029 (2002), arXiv:hep-ph/0204244.
[57] P. Nason, JHEP **11**, 040 (2004), arXiv:hep-ph/0409146.
[58] S. Frixione, P. Nason, and C. Oleari, JHEP **11**, 070 (2007), arXiv:0709.2092 [hep-ph].
[59] S. Alioli, P. Nason, C. Oleari, and E. Re, JHEP **06**, 043 (2010), arXiv:1002.2581 [hep-ph].
[60] S. Höche, F. Krauss, M. Schönherr, and F. Siegert, JHEP **04**, 024 (2011), arXiv:1008.5399 [hep-ph].
[61] S. Höche, F. Krauss, M. Schönherr, and F. Siegert, JHEP **09**, 049 (2012), arXiv:1111.1220 [hep-ph].
[62] J. Alwall, R. Frederix, S. Frixione, V. Hirschi, F. Maltoni, O. Mattelaer, H. S. Shao, T. Stelzer, P. Torrielli, and M. Zaro, JHEP **07**, 079 (2014), arXiv:1405.0301 [hep-ph].
[63] J. Andre and T. Sjöstrand, Phys. Rev. D **57**, 5767 (1998), arXiv:hep-ph/9708390.
[64] S. Catani, F. Krauss, R. Kuhn, and B. R. Webber, JHEP **11**, 063 (2001), arXiv:hep-ph/0109231.
[65] L. Lönnblad, JHEP **05**, 046 (2002), arXiv:hep-ph/0112284.
[66] M. L. Mangano, M. Moretti, and R. Pittau, Nucl. Phys. B **632**, 343 (2002), arXiv:hep-ph/0108069.
[67] F. Krauss, JHEP **08**, 015 (2002), arXiv:hep-ph/0205283.
[68] N. Lavesson and L. Lönnblad, JHEP **04**, 085 (2008), arXiv:0712.2966 [hep-ph].
[69] S. Höche, F. Krauss, S. Schumann, and F. Siegert, JHEP **05**, 053 (2009), arXiv:0903.1219 [hep-ph].
[70] K. Hamilton, P. Richardson, and J. Tully, JHEP **11**, 038 (2009), arXiv:0905.3072 [hep-ph].
[71] L. Lönnblad and S. Prestel, JHEP **03**, 019 (2012), arXiv:1109.4829 [hep-ph].
[72] L. Lönnblad and S. Prestel, JHEP **02**, 094 (2013), arXiv:1211.4827 [hep-ph].
[73] S. Plätzer, JHEP **08**, 114 (2013), arXiv:1211.5467 [hep-ph].
[74] S. Höche, J. Krause, and F. Siegert, Phys. Rev. D **100**, 014011 (2019), arXiv:1904.09382 [hep-ph].
[75] N. Lavesson and L. Lönnblad, JHEP **12**, 070 (2008), arXiv:0811.2912 [hep-ph].
[76] T. Gehrmann, S. Höche, F. Krauss, M. Schönherr, and F. Siegert, JHEP **01**, 144 (2013), arXiv:1207.5031 [hep-ph].
[77] S. Höche, F. Krauss, M. Schönherr, and F. Siegert, JHEP **04**, 027 (2013), arXiv:1207.5030 [hep-ph].
[78] R. Frederix and S. Frixione, JHEP **12**, 061 (2012), arXiv:1209.6215 [hep-ph].
[79] L. Lönnblad and S. Prestel, JHEP **03**, 166 (2013), arXiv:1211.7278 [hep-ph].
[80] S. Catani and M. H. Seymour, Nucl. Phys. B **485**, 291 (1997), [Erratum: Nucl.Phys.B 510, 503–504 (1998)], arXiv:hep-ph/9605323.
[81] S. Catani, S. Dittmaier, M. H. Seymour, and Z. Trocsanyi, Nucl. Phys. B **627**, 189 (2002), arXiv:hep-ph/0201036.
[82] A. Bassetto, M. Ciafaloni, and G. Marchesini, Phys. Rept. **100**, 201 (1983).
[83] S. Höche and M. Schönherr, Phys. Rev. D **86**, 094042 (2012), arXiv:1208.2815 [hep-ph].
[84] J. M. Campbell, S. Höche, M. Knobbe, C. T. Preuss, and D. Reichelt, (2025), arXiv:2505.10408 [hep-ph].
[85] M. Gell-Mann and M. L. Goldberger, Phys. Rev. **96**, 1433 (1954).
[86] L. S. Brown and R. L. Goble, Phys. Rev. **173**, 1505 (1968).
[87] T. Gleisberg and F. Krauss, Eur. Phys. J. C **53**, 501 (2008), arXiv:0709.2881 [hep-ph].
[88] S. Höche, S. Liebschner, and F. Siegert, Eur. Phys. J. C **79**, 728 (2019), arXiv:1807.04348 [hep-ph].
[89] S. Catani, Y. L. Dokshitzer, M. Olsson, G. Turnock, and B. R. Webber, Phys. Lett. B **269**, 432 (1991).
[90] G. Coloretti, A. Gehrmann-De Ridder, and C. T. Preuss, JHEP **06**, 009 (2022), arXiv:2202.07333 [hep-ph].
[91] J. Zhu, Y. Song, J. Gao, D. Kang, and T. Maji, Chin. Phys. C **49**, 023106 (2025), arXiv:2311.07282 [hep-ph].
[92] A. Gehrmann-De Ridder, C. T. Preuss, and C. Williams, JHEP **03**, 104 (2024), arXiv:2310.09354 [hep-ph].
[93] M. Knobbe, F. Krauss, D. Reichelt, and S. Schumann, Eur. Phys. J. C **84**, 83 (2024), arXiv:2306.03682 [hep-ph].
[94] B. Campillo Aveleira, A. Gehrmann-De Ridder, and C. T. Preuss, Eur. Phys. J. C **84**, 789 (2024), arXiv:2402.17379 [hep-ph].
[95] A. Gehrmann-De Ridder, C. T. Preuss, D. Reichelt, and S. Schumann, JHEP **07**, 160 (2024), arXiv:2403.06929 [hep-ph].
[96] E. Fox, A. Gehrmann-De Ridder, T. Gehrmann, N. Glover, M. Marcoli, and C. T. Preuss, Phys. Rev. Lett. **134**, 251905 (2025), arXiv:2502.17333 [hep-ph].
[97] T. Gleisberg, S. Höche, F. Krauss, A. Schälicke, S. Schumann, and J.-C. Winter, JHEP **02**, 056 (2004), arXiv:hep-ph/0311263.
[98] T. Gleisberg, S. Höche, F. Krauss, M. Schönherr, S. Schumann, F. Siegert, and J. Winter, JHEP **02**, 007 (2009), arXiv:0811.4622 [hep-ph].
[99] E. Bothmann *et al.* (Sherpa), SciPost Phys. **7**, 034 (2019), arXiv:1905.09127 [hep-ph].
[100] E. Bothmann *et al.* (Sherpa), JHEP **12**, 156 (2024), arXiv:2410.22148 [hep-ph].
[101] F. Krauss, R. Kuhn, and G. Soff, JHEP **02**, 044 (2002), arXiv:hep-ph/0109036.
[102] T. Gleisberg and S. Höche, JHEP **12**, 039 (2008), arXiv:0808.3674 [hep-ph].
[103] J. M. Campbell and R. K. Ellis, Phys. Rev. D **60**, 113006 (1999), arXiv:hep-ph/9905386.
[104] J. M. Campbell, R. K. Ellis, and C. Williams, JHEP **07**, 018 (2011), arXiv:1105.0020 [hep-ph].
[105] J. M. Campbell, R. K. Ellis, and W. T. Giele, Eur. Phys. J. C **75**, 246 (2015), arXiv:1503.06182 [physics.comp-ph].
[106] J. Campbell and T. Neumann, JHEP **12**, 034 (2019), arXiv:1909.09117 [hep-ph].
[107] J. M. Campbell, S. Höche, and C. T. Preuss, Eur. Phys. J. C **81**, 1117 (2021), arXiv:2107.04472 [hep-ph].

[108] F. Cascioli, P. Maierhofer, and S. Pozzorini, Phys. Rev. Lett. **108**, 111601 (2012), arXiv:1111.5206 [hep-ph].
[109] F. Buccioni, S. Pozzorini, and M. Zoller, Eur. Phys. J. C **78**, 70 (2018), arXiv:1710.11452 [hep-ph].
[110] F. Buccioni, J.-N. Lang, J. M. Lindert, P. Maierhöfer, S. Pozzorini, H. Zhang, and M. F. Zoller, Eur. Phys. J. C **79**, 866 (2019), arXiv:1907.13071 [hep-ph].
[111] S. Catani, B. R. Webber, and G. Marchesini, Nucl. Phys. B **349**, 635 (1991).
[112] A. Buckley, J. Butterworth, D. Grellscheid, H. Hoeth, L. Lönnblad, J. Monk, H. Schulz, and F. Siegert, Comput. Phys. Commun. **184**, 2803 (2013), arXiv:1003.0694 [hep-ph].
[113] C. Bierlich *et al.*, SciPost Phys. **8**, 026 (2020), arXiv:1912.05451 [hep-ph].
[114] C. Bierlich, A. Buckley, J. M. Butterworth, C. Gutschow, L. Lönnblad, T. Procter, P. Richardson, and Y. Yeh, SciPost Phys. Codeb. **36**, 1 (2024), arXiv:2404.15984 [hep-ph].
[115] D. Amati, A. Bassetto, M. Ciafaloni, G. Marchesini, and G. Veneziano, Nucl. Phys. B **173**, 429 (1980).
[116] J. Kodaira and L. Trentadue, Phys. Lett. B **112**, 66 (1982).
[117] C. T. H. Davies and W. J. Stirling, Nucl. Phys. B **244**, 337 (1984).
[118] C. T. H. Davies, B. R. Webber, and W. J. Stirling, **1**, I.95 (1984).
[119] S. Catani, E. D'Emilio, and L. Trentadue, Phys. Lett. B **211**, 335 (1988).
[120] A. Heister *et al.* (ALEPH), Eur. Phys. J. C **35**, 457 (2004).
[121] P. Pfeifenschneider *et al.* (JADE, OPAL), Eur. Phys. J. C **17**, 19 (2000), arXiv:hep-ex/0001055.
[122] G. Abbiendi *et al.* (OPAL), Eur. Phys. J. C **40**, 287 (2005), arXiv:hep-ex/0503051.
[123] E. Farhi, Phys. Rev. Lett. **39**, 1587 (1977).
[124] P. Nason and G. Zanderighi, JHEP **06**, 058 (2023), arXiv:2301.03607 [hep-ph].
[125] S. Catani and B. R. Webber, JHEP **10**, 005 (1997), arXiv:hep-ph/9710333.
[126] G. Abbiendi *et al.* (OPAL), Eur. Phys. J. C **20**, 601 (2001), arXiv:hep-ex/0101044.
[127] R. Frederix, S. Frixione, K. Melnikov, and G. Zanderighi, JHEP **11**, 050 (2010), arXiv:1008.5313 [hep-ph].